Journal of Low Temperature Physics
https://doi.org/10.1007/s10909-022-02790-0

Radio-Frequency Resonances and Damping in Metallic Magnetic Calorimeter Sensors

S. T. P. Boyd[1] · **G.-B. Kim**[2] · **S. Friedrich**[2]

Received: 1 November 2021 / Accepted: 13 May 2022

Abstract
Metallic magnetic calorimeters (MMCs) are particle detectors that combine ultra-high energy resolution with a predictable and smooth response based on the physics of paramagnetism. For best energy resolution, MMCs are read out with dc SQUID preamplifiers. Since the ac Josephson effect also makes dc SQUIDs broadband RF sources in the 1–100 GHz range, the SQUID can potentially excite RF modes of the MMC sensor, with negative consequences. The importance of this possibility is magnified in direct-coupled MMCs, where the MMC sensor is part of the SQUID loop to maximize performance. For these reasons, the RF behavior of MMC sensors must be investigated. In this report, we present the results of exploratory RF simulations of MMC sensor modes and damping, and we assess three approaches to damp the parallel-meander direct-coupled MMC without excessive noise increase.

Keywords Metallic magnetic calorimeter · MMC · RF simulation

1 Introduction

Metallic magnetic calorimeters (MMCs) [1–3] are particle detectors that combine ultra-high resolving power of up to ~6000 [4] with a predictable and smooth response [5] based on the physics of paramagnetism. This makes MMCs the best candidates for many precision radiation measurements.

To achieve the highest possible energy resolution, MMCs are read out with dc SQUID preamplifiers. Because of the ac Josephson effect and nonlinear interaction of the two interfering Josephson junctions, dc SQUIDs are also broadband RF generators in the 1–100 GHz range [6]. They can thus excite RF modes of the MMC sensors, with the potential to cause non-smooth SQUID characteristics, heat

✉ S. T. P. Boyd
stpboyd@gmail.com

[1] University of New Mexico, Albuquerque, NM 87131, USA

[2] Lawrence Livermore National Laboratory, Livermore, CA 94550, USA

Published online: 20 July 2022

the sensors, induce currents that may impact persistent current trapping, and cause unwanted interaction among multiple MMCs on a chip.

The potential importance of MMC sensor RF modes has increased recently with work in design and measurement of direct-coupled MMCs [7–9]. This work has used a parallel-meander geometry for the sensor: the upper meander, just below the paramagnet, is part of the SQUID loop for maximum sensitivity, while the lower meander carries the relatively large ~100 mA magnetizing current. This parallel-meander geometry is expected to exhibit high-Q RF resonances, and in fact non-smooth I-V behavior and intrinsic SQUID resonances have been reported [9].

It is thus increasingly important to understand the RF modes and damping of MMC sensors. In this report, we present the results of exploratory RF simulations of MMC sensors and assess several schemes to damp resonances in the parallel-meander geometry without creating excessive noise.

2 Modeling Approach and Geometry

RF simulations were performed using finite element simulations in 3D and 2D slab geometries with commercial software [10]. Most 3D geometries were modeled in a 250 μm-radius sphere surrounded by a perfectly matched layer. The background dielectric constant was set to 5 to avoid meshing thin layers of SiO_2, and loss tangent was set to 10^{-3}. These choices reduced the problem size, avoided cavity modes, and limited the maximum Q factor to 1000. Superconducting meanders were modeled as perfectly conducting 2D boundaries, also to reduce the problem size. Our testing indicates that this simplification typically causes inductance errors of ~ 15%–20%. The normal-conducting resistors, damping layers and paramagnet (PM) were 3D structures. The PM was modeled as normal-conducting metal, without including magnetic behavior in this exploratory study. The meander geometry was typical for MMCs, with 5 μm wide traces on a 10 μm pitch and boundaries 5 μm inside the 260 μm × 265 μm × 1.5 μm thick PM. The meander was 6.5 mm long with a 2.0 nH inductance. The straight sections of the meander were aligned with the y-axis, and the z-axis was normal to the surface of the wafer.

3 Simulations and Discussion

We initially modeled an isolated meander as a reference case. It displayed a chain of high Q resonances that can be classified into wavelengths λ by the pattern of the x-component of the electric field E_x (Fig. 1 *Left*). The lowest mode seen (1λ) was at 63 GHz. After we quadrupled the area of the meander, the lowest mode dropped to 23 GHz. It is noteworthy that in real devices the Q values of these modes could potentially be very high, as they are limited only by dielectric loss and radiation.

We next modeled a basic MMC sensor by putting a PM 300 nm above the meander. This normal-metal overlayer eliminated the high-Q isolated-meander modes but created a new set of microstrip modes (Fig. 1 *Right*). These modes have not created difficulty for most MMCs because, fortuitously, the typical residual-resistivity ratio

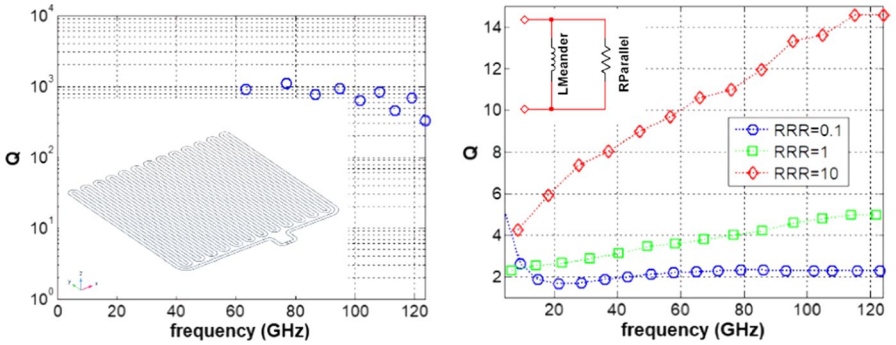

Fig. 1 *Left* Resonance spectrum for an isolated meander. The inset shows the meander geometry. *Right* Resonance spectra for the meander with PM above it for three values of PM *RRR*. The inset shows the electrical schematic used to model the low-frequency white noise from R_{parallel}. (Color figure online)

$(RRR) = 2$ for sputtered Au damps the modes well. Note also that although high conductivity of the PM might be desirable, *e.g.,* to reduce signal rise times, it would also reduce microstrip mode damping because of the skin effect.

From the fluctuation–dissipation theorem [11], this damping must create noise. We calculated the flux noise at the sensor as

$$S^{1/2}_{\text{damping}} = \frac{L_{\text{meander}}}{\phi_0}\sqrt{\frac{4k_{\text{B}}T}{R_{\text{parallel}}}},\ \text{with} R_{\text{parallel}} = \frac{V^2_{\text{meander}}}{P_{\text{total}}}$$

with k_{B} the Boltzmann constant, ϕ_0 the flux quantum, and T the reference noise temperature 0.1 K used throughout this report. The meander self-inductance L_{meander}, the total dissipated power P_{total}, and the voltage across the meander V_{meander} were determined from frequency-domain simulations. We find a low-frequency noise of 0.20, 0.64, and 2.0 $\mu\phi_0/\text{Hz}^{1/2}$ for $RRR = 0.1$, 1, and 10. For direct-coupled MMCs, this flux noise can be compared to typical SQUID flux noise ~1 $\mu\phi_0/\text{Hz}^{1/2}$. For transformer-coupled MMCs, it should be compared to the optimal effective SQUID noise at the sensor of ~11 $\mu\phi_0/\text{Hz}^{1/2}$.

To investigate direct-coupled MMCs, we added a second meander below the first. As expected, a new set of high-Q microstrip modes appears between the two meanders (Fig. 2 *Left*). Q values range from 200–500, showing the new modes couple only weakly to the PM for the *RRR* values of 0.1, 1, and 10 that we have investigated. For best functioning of direct-coupled MMCs, it is imperative to increase the damping of these new modes, and to do so without adding excessive noise.

The simplest approach to damp the new modes of the parallel-meander geometry is to put a resistor R_{Damping} across one or both meanders. Simulations with $RRR = 1$ using $R_{\text{Damping}} = 10\Omega$ and 100Ω are shown in Fig. 2 (*Right)*. The resistor was placed across the lower meander; placing it across the upper meander creates negligible damping. However, of the new modes, only those with half-integer wavelengths were damped, because only those modes couple to R_{Damping}. The damping increase in the step from 100Ω to 10Ω was significant, but the increase from 10Ω to 1Ω (not

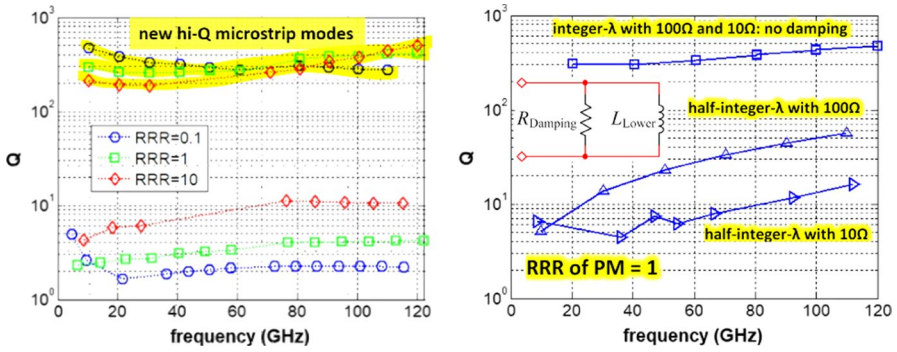

Fig. 2 *Left* Resonance spectra for a parallel-meander geometry below the paramagnet for $RRR = 0.1$, 1, and 10, showing new high-Q microstrip modes between the two meanders. *Right* Resonance spectra for the new modes only, with damping resistor $R_{\text{Damping}} = 100\Omega$ and 10Ω. Only half of the new modes, those with half-integer wavelengths, can be damped. (Color figure online)

shown) was slight. The integer-wavelength Q values that are not damped by R_{Damping} differ slightly from Fig. 2 (*Left)* because the assumed insulating layer thicknesses were slightly different. We estimate the noise at the sensor to be 0.66 $\mu\phi_0/\text{Hz}^{1/2}$ and 0.91 $\mu\phi_0/\text{Hz}^{1/2}$ for $R_{\text{Damping}} = 100\Omega$ and 10Ω, respectively.

It may be possible to improve the damping that can be obtained with resistors, *e.g.,* by putting additional resistors between the turns of the meander, and we simulated some designs of this type. However, it appears to be simpler and more effective to employ distributed damping via either a damping layer or a lossy transmission line.

To create a damping layer, a rectangle of normal-conducting metal, the same size as the PM, is deposited between the two meanders. This layer should be electrically isolated. A damping layer shorted to either meander results in a R_{parallel} with very low resistance and creates high current noise and low roll-off frequency in both meanders. Thus the damping layer fabrication process requires an additional insulating layer compared to resistor damping.

A simulation assuming a 1 μm-thick isolated damping layer of Au with $RRR = 1$ shows that Q is now strongly reduced for *all* modes in the frequency range of interest, with a maximum $Q \approx 5$ and a simple resonance structure (Fig. 3 *Left*). The two branches of $Q(f)$ found in this simulation correspond to whether the stripline mode (upper meander) is in phase or in antiphase with the microstrip mode (lower meander). We estimate the noise at the sensor in this configuration to be 0.82 $\mu\phi_0/\text{Hz}^{1/2}$. The damping layer geometry appears to be strongly preferable to the 10 Ω resistor, as all the modes are damped, and to lower Q, while contributing less noise.

Can we do better than the damping layer? As a simplifying alternative, we can view the meander pair as a meander of a lossy transmission line (TL). Such a geometry should reduce noise compared to the unpatterned damping layer by eliminating large normal-conducting loops.

The behavior of a lossy transmission line is readily obtained from finite-element simulations in 2D slab geometry, which converge quickly compared to the

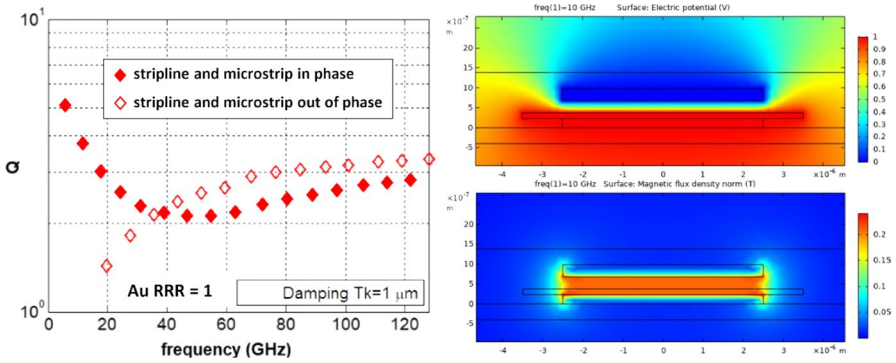

Fig. 3 *Left:* Resonance spectrum for the isolated damping layer. In contrast to resistor damping, all modes are now strongly damped. *Right:* Example electric (upper) and magnetic field (lower) 2D solutions of a lossy TL. The superconducting traces are 5 μm wide, with thickness 230 nm for the lower and 400 nm for the upper trace. The damping trace is 7 μm wide, and in these views is 150 nm thick. (Color figure online)

3D case (Fig. 3 *Right*). The distributed inductance, capacitance, resistance, and conductance L, C, R, and G of the TL are calculated, and from these parameters the attenuation constant (number of $1/e$ lengths per meter) versus frequency and geometry can be assessed (Fig. 4 *Left*) [12].

3D simulations for the lossy-TL geometry assuming a 1 μm-thick Au damping layer with $RRR = 1$ show strong damping of all modes (Fig. 4 *Right*), and an estimated noise of 0.63 $\mu\phi_0/\mathrm{Hz}^{1/2}$. It is noteworthy that there is no resolvable noise penalty for this damping approach within our calculation accuracy. The noise is also quite insensitive to the damping layer thickness.

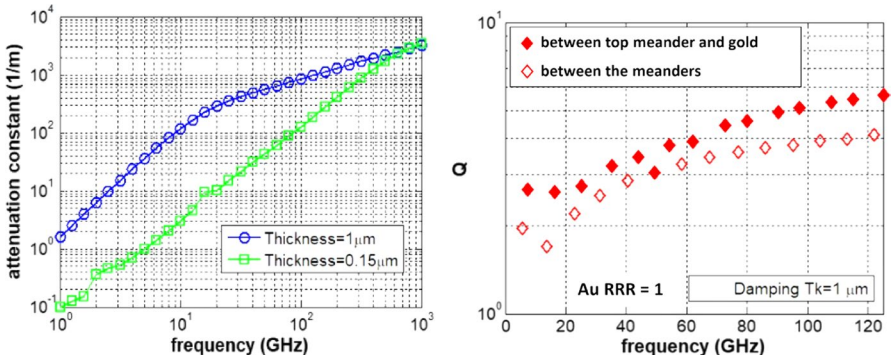

Fig. 4 Lossy transmission line (TL) approach. *Left* the attenuation constant versus frequency for two different thicknesses of the damping layer, which is assumed to be Au with $RRR = 1$. *Right* Resonance spectrum with the lossy TL approach with a damping layer thickness of 1 μm. (Color figure online)

4 Conclusions

A superconducting meander coil in isolation supports modes which can reach very high Q. These modes can be damped effectively by an isolated overlayer of normal metal such as an MMC paramagnet (PM). For gradiometric single-layer MMC sensors with large meanders, but with PM only on one side, *e.g.,* sensors used for thermometry or testing $M(T)$ curves, it may be prudent to put a normal-metal film on the non-PM side to damp these modes.

Placing a PM on top of a single-layer meander to create an MMC sensor eliminates the isolated-meander modes but creates a new set of microstrip modes. These microstrip modes have not been a problem for MMC research to date because, fortuitously, typical PM $RRR \approx 2$ provides good damping.

The direct-coupled parallel-meander geometry creates new high-Q microstrip modes between the meanders. These new modes couple only weakly to the PM damping. We find that good damping of these new modes across the 1 GHz–100 GHz range can be achieved with no resolvable noise penalty by configuring the meander pair as a lossy transmission line. We find that typical sputtered Au with $RRR \approx 2$ achieves good damping in this configuration with a 1 μm thickness.

Acknowledgements This work was funded by the National Nuclear Security Administration of the Department of Energy, Office of International Nuclear Safeguards. It was performed under the auspices of the U.S. DOE by LLNL under Contract No. DE-AC52-07NA27344. • Data used in this work will be made available upon reasonable request. • LLNL-JRNL-828692

References

1. A. Fleischmann, C. Enss, G. Seidel, in *Metallic Magnetic Calorimeters*, ed. by C. Enss, K. Irwin. Cryogenic Particle Detection. Topics Appl. Phys., Vol 99. (Springer, Berlin) https://doi.org/10.1007/10933596_4
2. A. Fleischmann et al., AIP Conf. Proc. **1185**, 571 (2009). https://doi.org/10.1063/1.3292407
3. S. Kempf, A. Fleischmann, L. Gastaldo, C. Enss, J. Low Temp. Phys. **193**, 365 (2018). https://doi.org/10.1007/s10909-018-1891-6
4. T. Sikorsky et al., Phys. Rev. Lett. **125**, 142503 (2020). https://doi.org/10.1103/PhysRevLett.125.142503
5. C.R. Bates et al., Appl. Phys. Lett. **109**, 023513 (2016). https://doi.org/10.1063/1.4958699
6. J. Clarke, A.I. Braginski (eds.), *The SQUID Handbook: Fundamentals and Technology of SQUIDs and SQUID Systems*, (Wiley-VCH, 2004). ISBN-13: 978–3527402298
7. S.T.P. Boyd et al., J. Low Temp. Phys. **199**, 681–687 (2020). https://doi.org/10.1007/s10909-020-02406-5
8. M. Krantz et al., IEEE Intl. Supercond. Electr. Conf. (ISEC) **2019**, 1 (2019). https://doi.org/10.1109/ISEC46533.2019.8990913
9. M. Krantz, Ph.D. Dissertation, University of Heidelberg, Germany, (2020). DOI: https://doi.org/10.11588/heidok.00028776
10. COMSOL Multiphysics® v.5.6. http://www.comsol.com. COMSOL AB, Stockholm, Sweden
11. H.B. Callen, T.A. Welton, Irreversibility and generalized noise. Phys. Rev. **83**, 34–40 (1951). https://doi.org/10.1103/PhysRev.83.34
12. D.M. Pozar, *Microwave Engineering*, 4th edn. (Wiley, Hoboken, NJ, 2012). (**ISBN-13: 978-0470631553**)